Double-phase hydride forming compounds : a new class of highly electrocatalytic materials

17. R. Barnard, C. F. Randell, and F. L. Tye, *J. Appl. Electrochem.*, **11**, 517 (1981).
18. G. Davolio and E. Soragni, *Electrochim. Acta*, **28**, 335 (1985).
19. D. L. Britton, in "Nickel Hydroxide Electrodes," D. A. Corrigan and A. H. Zimmerman, Editors, PV 90-4, p. 233, The Electrochemical Society Softbound Proceedings Series, Pennington, New Jersey (1990).

Double-Phase Hydride Forming Compounds: A New Class of Highly Electrocatalytic Materials

P. H. L. Notten and P. Hokkeling

Philips Research Laboratories, 5600 JA Eindhoven, The Netherlands

ABSTRACT

A new class of materials is proposed to improve the electrocatalytic activity of hydride forming intermetallic compounds of the AB_5-type without making use of highly electrocatalytic precious metals like Pd or Pt. These materials, denoted as $AB_{5.5}$, consist of two different crystallographic phases: the bulk phase, still responsible for hydrogen storage, is formed by the corrosion-resistant multicomponent "standard alloy" based on $LaNi_5$; and a second phase, homogeneously decorating the surface of the bulk-phase particles, provides for the extremely fast electrochemical hydrogen reaction. The composition of the second-phase alloy is such that synergism in the electrocatalysis occurs. A simple metallurgical method of producing double-phase materials is described. Various analytical techniques such as EPMA and x-ray diffraction are employed to characterize the solids produced. It is shown that the kinetics of the charge-transfer reaction can be characterized electrochemically by the overall exchange current. In accordance with the Brewer-Engel theory, $MoCo_3$ precipitates are found to be highly electrocatalytic, which is reflected in an increase of the overall exchange current from 190 $mA \cdot g^{-1}$ for the single-phase AB_5 compound to 588 $mA \cdot g^{-1}$. As a consequence very high discharge efficiencies are accomplished with these $MoCo_3$-based powder electrodes, even under extreme conditions: at 0°C the efficiency is improved from 34 to 90%.

The absorption of large amounts of hydrogen gas by binary intermetallic compounds was first observed on $SmCo_5$ by Zijlstra and Westendorp about two decades ago (1). Since then, other intermetallic compounds such as $LaNi_5$, generally denoted as AB_5 compounds, were also found to absorb and release hydrogen gas in large quantities (2-4). Similarly, electrolytically made hydrogen can be stored in electrodes made of these materials. The reverse reaction, *i.e.*, the oxidation of atomic hydrogen, is also possible. This reversible behavior in combination with the large storage capacity makes these electrodes, in principle, very attractive as negative electrodes in a new generation of rechargeable batteries (5, 6). In particular the nontoxic properties of the chemical elements from which these hydride forming materials are composed are a great environmental advantage in comparison with cadmium, nowadays commonly employed as negative electrode material in secondary Ni/Cd cells.

The corrosion stability (S) of the above-mentioned binary compounds in contact with aqueous solutions is, however, rather poor. For example, when a $LaNi_5$ electrode is successively charged and discharged 400 times, more than 80% of the hydride forming material has become inactive. The stability after this cycle number [$S(400)$] has been expressed in terms of a capacity ratio according to

$$S(400) = \frac{C_t(400)}{C_t(0)} \times 100\% \qquad [1]$$

where $C_t(0)$ and $C_t(400)$ represent the initial total storage capacity, determined from extrapolation to the zeroth cycle, and the remaining total storage capacity after 400 cycles, respectively (7). A value of 12% for $S(400)$ was measured on $LaNi_5$ electrodes. Willems *et al.* (7, 8) have shown by x-ray diffraction analyses and electron microscopy that corrosion products such as $La(OH)_3$ are increasingly formed during prolonged cycling. They also showed that the stability of $LaNi_5$ can be significantly improved when part of the Ni and/or La in the solid is replaced by other elements. The reported Ni-substituted ternary systems are listed in Table I. A further improvement was achieved by the addition of small amounts of either Si or Al. The results of the Si-based quaternary systems are also listed in this table. The increase of the corrosion stability up to 96% with decreasing Ni content was attributed to a reduction of the crystal lattice expansion during hydrogen cycling (7, 8).

Though essential, the corrosion resistivity is not the only aspect which has to be taken into account with regard to the good functioning of hydride forming electrodes. Other important properties are, for example, the initial storage capacity, the attainable charge and discharge rate, and the rate at which freshly prepared electrodes can be activated. It was found that these important electrode characteristics also strongly depend on the composition of the intermetallic compound (7-9). On the basis of the above considerations it was concluded that a pentary AB_5 system with composition $La_{0.8}Nd_{0.2}Ni_{2.5}Co_{2.4}Si_{0.1}$ (see Table I) was most suitable for the application in rechargeable batteries (7, 8). In this work we will therefore consider this single-phase compound as "the standard alloy."

A disadvantage of the substituted materials is, however, that this simultaneously results in a substantial decrease of the kinetics of the electrochemical hydrogen reaction. In recent work we have shown that the catalytic activity can be restored by replacing small amounts of Co by more electrocatalytic elements such as Pd or Pt (9). A simple additional model was shown to be valid which takes the electrocatalytic activity of the individual elements into account. One important drawback of this procedure is that

Table I. The corrosion stability [$S(400)$] of various multicomponent hydride forming AB_5 systems [from Ref. (7)].

	AB_5 compound	$S(400)$ (%)
Binary system	$LaNi_5$	12
Ternary systems	$LaNi_4Co_1$	25
	$LaNi_3Co_2$	30
	$LaNi_{2.5}Co_{2.5}$	45
	$LaNi_2Co_3$	61
Quaternary systems	$LaNi_4Co_1Si_{0.1}$	33
	$LaNi_3Co_2Si_{0.1}$	65
	$LaNi_{2.5}Co_{2.5}Si_{0.1}$	81
	$LaNi_2Co_3Si_{0.1}$	96
Pentary system (standard alloy)	$La_{0.8}Nd_{0.2}Ni_{2.5}Co_{2.4}Si_{0.1}$	86

by solidifying a homogeneous melt the precious metals are distributed throughout the solid, whereas the metals assert their advantageous influence at the surface of the powdered solid only.

Another elegant approach was adopted by Jakšić and co-workers (10-13). They have extensively described that the kinetics of the hydrogen evolution reaction can also be remarkably improved when the appropriate combinations of transition metals are employed. Referring to the Brewer-Engel valence bond theory they pointed out that so-called synergistic effects in the electrocatalysis might be theoretically expected when transition metals having vacant d-orbitals are alloyed with metals having internally paired d-electrons. As a result of the interaction of both metals an optimum electron configuration for the hydrogen reaction to occur can be adjusted which exceeds the electrocatalytic activity of the individual elements and, in some cases, might even exceed that of precious metals. It was argued that binary compounds such as $MoCo_3$, $MoNi_3$, and WNi_3 are the most promising alloys (11-13). After galvanic codeposition of small amounts of Mo and Co onto various substrates, Lačnjevac *et al.* (10, 12) indeed found in their experiments that the overpotentials for the hydrogen evolution reaction were dramatically reduced over the entire current density range and were even lower than those found at Pt electrodes. Synergistic effects were also reported for binary alloys of nickel and cobalt (14).

The aim of the work described in this paper was to improve the kinetics of the electrochemical hydrogen reaction at the substituted AB_5 alloys, in particular the corrosion-resistant standard alloy (see Table I), by making use of the reported "synergistic compounds." Since these compounds only need to be available at the surface of the hydride forming powder, *in situ* galvanic codeposition also seems to be attractive in the present case. However, as a homogeneous distribution of the highly catalytic precipitates over the entire powder surface is far more difficult to achieve with porous electrode systems than on flat surfaces we adopted a different, but even simpler, approach. We tried to modify the composition of the melt in such a way that during the solidification process a double-phase system is formed which consists of the hydride forming standard alloy and a second catalytic phase, decorating the powder surface. In the following Theoretical section we will show how this can easily be achieved.

The kinetics of the electrochemical hydrogen reaction are generally characterized by the exchange current density (15-17). In order to judge the electrocatalytic activity of the various intermetallic compounds we similarly determined this parameter. The processes occurring at the double-phase electrodes are also considered in the Theoretical section together with the factors affecting the exchange current.

Two different systems, both based on the standard alloy as hydride forming compound, were investigated. The second phase was formed either by a Ni/Co alloy or a Mo/Co alloy. Preceding the electrochemical measurements on powder electrodes, *i.e.*, determination of the exchange current, discharge efficiency at low temperature and cycle life, the phase distribution, and their composition in the solid samples were analyzed both qualitatively and quantitatively using optical microscopy, scanning electron microscopy in combination with electron probe microanalysis, and x-ray diffraction.

Theoretical Considerations

On the basis of the well-known phase diagram of the La/Ni system, which is partly shown in Fig. 1, we will demonstrate how in principle double-phase structured solids can be formed during the solidification process. It was shown by Buschow *et al.* (18) that a relatively large homogeneity region exists for the $LaNi_5$ compound. Thus single-phase AB_5-related solids are obtained when the Ni content ranges from 4.8 to 5.4 (see shaded region in Fig. 1). When a homogeneous melt with higher Ni content (>5.4) is cooled down, the initially formed AB_5 compound is in contact with a Ni-enriched liquid. Approaching the eutectic temperature (T_e) the grown AB_5 crystallites are in equilibrium with the surrounding liquid having the eutectic composition. A further temperature decrease completes the solidification process and ultimately results in AB_5 crystallites which are decorated with pure Ni precipitates at the grain boundaries. Obviously, with regard to the hydrogen storage capacity it is desirable that the ratio between the amount of hydride forming AB_5 compound and that of the precipitates should be as large as possible. We therefore suggest the use of an overall melt composition of $AB_{5.5}$, a composition just outside the homogeneity region. Although the phase diagrams for more complicated systems are unknown, we employed this principle in the present study to decorate the standard alloy crystallites with a second, highly electrocatalytic, phase. Which alloy composition will be formed from the multicomponent containing melt depends, of course, on the thermodynamic stability of the second phase. Advantageously, it was argued that there exists a direct correlation between the thermodynamic stability of these alloys and their electrocatalytic activity, which would imply that formation of the desired alloy may be expected (13). Furthermore, it is well known that grain boundaries are, in general, the weak pathways within a solid. It seems therefore likely that when the as-produced double-phase solids are pulverized, either by hydrogen gas absorption or by mechanical grinding, the precipitates are located at the exterior of the powder particles.

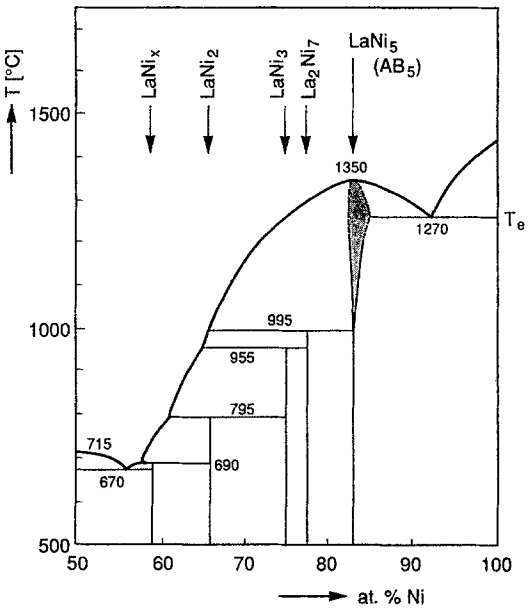

Fig. 1. Phase diagram of the Ni-rich part of the binary La/Ni system. The homogeneity region of $LaNi_5$ is indicated (lightly shaded). T_e represents the eutectic temperature. From Ref. (18).

A schematic representation of an electrode composed of a double-phase $AB_{5.5}$ powder in contact with an alkaline solution is shown in Fig. 2. The hydride forming AB_5 compound is denoted as phase I, whereas the second synergistic compound (lightly shaded) is indicated by phase II. For simplicity it is assumed that the porous electrode consists of spherical particles. Furthermore, it is assumed that all particles make contact with neighboring particles, so that the electrical resistance within the electrode is negligibly low and, consequently, electron transport can undisturbedly proceed. The various processes which must be considered during the electrochemical hydrogen reaction are also indicated in Fig. 2. When we restrict ourselves, for the moment, to processes occurring at phase I, the following steps can be successively distinguished during the reduction reaction

1. The supply of reactants by means of (convective) diffusion from the bulk of the electrolyte to the solid/solution interface I, indicated by the subscripts (b) and s(I), respectively

$$H_2O_b \rightleftarrows H_2O_{s(I)} \qquad [2]$$

2. The charge-transfer reaction occurring at the interface, which can be represented in alkaline solution by

$$H_2O_{s(I)} + e^- \underset{k_a}{\overset{k_c}{\rightleftarrows}} H_{ad(I)} + OH^-_{s(I)} \quad [3]$$

where k_c and k_a are the reaction rate constants for the reduction and oxidation reaction, respectively. As a result of the reduction reaction, atomic hydrogen (H_{ad}) is chemically adsorbed on the surface of phase I.

3. The removal of the electrochemically formed reaction products from the interface by means of diffusion. This includes the absorption of the adsorbed hydrogen by the AB_5 compound (H_{abs}) through which a hydride is formed

$$H_{ad(I)} \underset{k_2}{\overset{k_1}{\rightleftarrows}} H_{abs} \quad [4]$$

and transport of OH^- into the bulk of the electrolyte

$$OH^-_{s(I)} \rightleftarrows OH^-_b \quad [5]$$

4. Depending on the hydrogen concentration in the solid either an α phase or a β hydride phase in equilibrium with the α phase is formed (3)

$$H_{abs(\alpha)} \rightleftarrows H_{abs(\beta)} \quad [6]$$

5. Finally, recombination of two H_{ad} atoms has to be taken into account. This leads to the formation of H_2 which is released from the surface as a gas

$$2H_{ad(I)} \rightarrow H_2 \uparrow \quad [7]$$

Whether this side-reaction (Eq. [7]) takes place after the absorption process (Eq. [4]) is completed or both reactions occur simultaneously, depends on the thermodynamic properties of the hydride forming intermetallic compound (7).

Evidently, the reverse reactions take place with the exception of Eq. [7], when the oxidation reaction is considered instead of the reduction process. In order to reduce the complexity of characterizing the kinetics of the hydride forming reaction we consider, for the moment, only the α phase. Furthermore, the hydrogen evolution reaction can be easily avoided under certain conditions. We will come back to this point in the Experimental section. The reactions represented by Eq. [6] and [7] are therefore omitted in the following mathematical derivation.

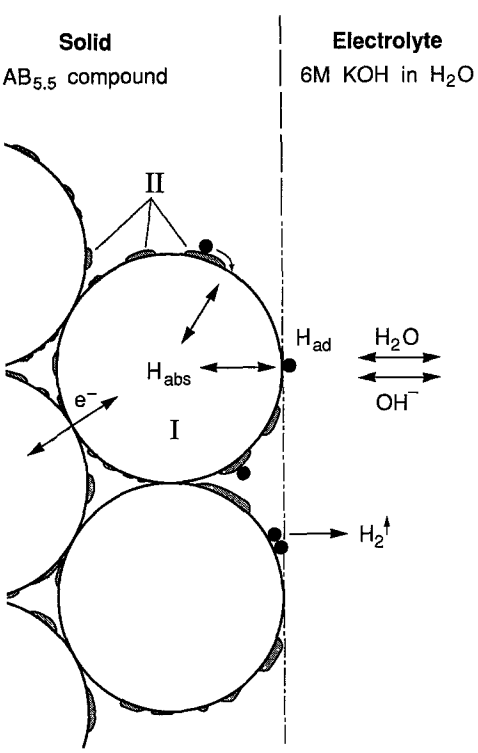

Fig. 2. Configuration of a double-phase $AB_{5.5}$ powder electrode in contact with an electrolyte of 6M KOH in water. The double-phase solid consists of a hydride forming intermetallic phase I of the AB_5 type and of a highly electrocatalytic phase II (lightly shaded) decorating the exterior of the powder surface, which provides for a fast electrochemical charge-transfer reaction. The various processes described in the text are indicated.

For a one-electron transfer reaction like that given by Eq. [3] the kinetics of the partial oxidation and partial reduction reaction can be represented by

$$I_a = FAk_a\theta^x a^y_{OH^-} \cdot \exp\left\{\frac{\alpha FE}{RT}\right\} \quad [8]$$

and

$$I_c = -FAk_c(1-\theta)a^z_{H_2O} \cdot \exp\left\{\frac{-(1-\alpha)FE}{RT}\right\} \quad [9]$$

where F is the Faraday constant; the surface coverage θ is a measure for the amount of the chemically adsorbed hydrogen: a_{OH^-} and a_{H_2O} are the activities of the indicated electroactive species at the solid/solution interface; x, y, and z are the reaction orders of H_{ad}, OH^-, and H_2O, respectively; α is the charge-transfer coefficient, in general, a constant having a value between 0 and 1; R is the gas constant; T is the absolute temperature, and E is the electrode potential. As in the case of the electrode charge capacity, it is more relevant for energy storage applications to refer to currents normalized per unit of weight instead of current densities. The specific surface of the powder electrode, A ($cm^2 \cdot g^{-1}$), was therefore introduced in Eq. [8] and [9] and both the partial anodic (I_a) and cathodic (I_c) currents are then expressed in $mA \cdot g^{-1}$. The exchange current I_o is defined at the equilibrium potential, E_e, where the external current is zero, *i.e.*, when I_a is equal to $-I_c$. From Eq. [8] and [9] it follows that under this condition I_o can be represented by

$$I_o = FAk_a\theta^x a^y_{OH^-} \cdot \exp\left\{\frac{\alpha FE_e}{RT}\right\} \quad [10]$$

$$= FAk_c(1-\theta)\, a^z_{H_2O} \cdot \exp\left\{\frac{-(1-\alpha)FE_e}{RT}\right\} \quad [11]$$

An expression for E_e can be obtained from Eq. [10] and [11]

$$E_e = \frac{RT}{F} \cdot \ln\left\{\frac{k_c(1-\theta)a^z_{H_2O}}{k_a\theta^x a^y_{OH^-}}\right\} \quad [12]$$

Eliminating E_e in Eq. [10], using Eq. [12], ultimately leads to a general expression for I_o according to

$$I_o = FAk_a^{(1-\alpha)}k_c^\alpha\theta^{x(1-\alpha)}(1-\theta)^\alpha a^{y(1-\alpha)}_{OH^-}a^{\alpha z}_{H_2O} \quad [13]$$

Similar concentration-dependent expressions for simple charge-transfer reactions were reported by Erdey-Grüz [page 53 of (19)] and Yayama *et al.* (20). They did not consider, however, the influence of electrode blocking on I_o by chemically adsorbed species involved in the electrochemical reaction. It is evident that in contrast to the H_{ad} activity, the H_2O and OH^- activities at the interface hardly change during the charge-transfer reaction as very strong alkaline (KOH) solutions are used in the present study. These surface concentrations remain equal to their bulk concentrations and, for a given electrolyte composition, can therefore be regarded as a constant. When, in addition, the reaction rate constants are combined, Eq. [13] can be simplified to

$$I_o = KAk\theta^{x(1-\alpha)}(1-\theta)^\alpha \quad [14]$$

where $K = Fa^{y(1-\alpha)}_{OH^-}a^{\alpha z}_{H_2O}$ and the combined rate constant k is given by $k_a^{(1-\alpha)}k_c^\alpha$. From the potential-independent relation of Eq. [14] it is obvious that I_o depends not only on the specific surface area and the reaction rate constant but also on the surface coverage by atomic hydrogen.

According to Eq. [4] a chemical equilibrium exists between the hydrogen stored in the solid and that adsorbed

on the electrode interface under the equilibrium conditions where I_o is defined. Assuming first-order kinetics for both the adsorption and desorption reaction and assuming that hydrogen adsorption takes place at discrete sites and that lateral interaction between the adsorbed species is absent, using the reaction rate constants given in Eq. [4], the relation between H_{ad} and H_{abs} is of the following form

$$\theta = \frac{[H_{abs}]}{[H_{abs}] + k_1/k_2} \quad [15]$$

This equation is very similar to the Langmuir adsorption isotherm [page 155 of (21)]. Obviously, the amount of adsorbed hydrogen which is expressed by θ depends on the rate constants for the absorption process. This shows that the kinetics of the charge-transfer reaction which is represented by I_o in Eq. [14], is related to the kinetics of the hydride forming process. Furthermore, Eq. [15] reveals that θ depends on the concentration of hydrogen within the solid. Although it is not definitely clear whether the above assumptions, and thus the above relationship is operative, other adsorption isotherms might be more successfully applied (21); they all show, however, a concentration dependence of θ. In order to eliminate this influence on I_o the hydrogen content stored in the AB_5 compound must be kept at a constant value in the experiments.

So far, the characterization of the kinetics was restricted to the hydride forming phase I. An equation similar to Eq. [14] can also be applied for phase II. Assuming that both phases do not influence each other, it is evident that both compounds contribute to the overall electrocatalytic activity of the double-phase material and consequently to the overall exchange current. A simple additional model leads to the following relationship for I_o

$$I_o = K_I A_I k_I \theta_I^{x(1-\alpha)}(1 - \theta_I)^{\alpha} + K_{II} A_{II} k_{II} \theta_{II}^{x(1-\alpha)}(1 - \theta_{II})^{\alpha} \quad [16]$$

where the subscripts I and II refer to the two phases considered above (see Fig. 2). It should be noted that the values for the constants x and α might be different for the two crystallographic phases. Clearly, the overall I_o depends on the relative magnitude of the surface areas of both phases and on their electrocatalytic activities.

It should be emphasized that when the hydrogen content within the solid is increased the β modification of the phase I compound is formed having its own characteristic rate constants. In that case a third additional term, taking this β phase into account, has to be added to Eq. [16]. Herewith it is assumed that the crystallographic-phase transition (Eq. [6]) is not rate determining. It has long been recognized that the β phase is in equilibrium with the α phase in a broad α to β conversion region which is characteristic for AB_5 hydride-forming materials (3). When the amount of absorbed hydrogen in the solid is increased in this conversion region the concentration of hydrogen in each phase remains essentially constant. This implies that under equilibrium conditions when both the α and β phase are present at the electrode surface the corresponding thetas should remain constant as well. What is actually changing is the relative amounts of each hydride phase. As a consequence, the relative magnitude of the surface areas of both hydride phases determines the phase I contribution to I_o in this conversion region. It has been argued that the surface composition under nonequilibrium conditions is dependent on whether the electrode is charged or discharged: during charging the electrode surface consists mainly of the β phase while it consists mainly of the α phase during discharging (7). According to the above reasoning this would obviously affect the electrode kinetics.

With regard to phase II it should be noted that this solid does not necessarily have to absorb the electrochemically formed hydrogen. It can be calculated, using Miedema's model (4), that hydride formation under moderate conditions is thermodynamically unfavorable for the phase II alloys considered in this work. This implies, for example, for the reduction reaction that the electrogenerated H_{ad} atoms must be transported along the phase II surface in order to form a hydride at phase I. This process is also indicated in Fig. 2. Such a mechanism, in which lateral diffusion of H_{ad} is essential under nonequilibrium conditions, was suggested to occur at "$LaNi_5$" by Wallace *et al.* (22). On the basis of their experiments they concluded that due to the very high lateral mobilities along the Ni precipitates formed outside the $LaNi_5$ powder particles, the surface reaction is rate determining. Similar results are reported for other hydride forming compounds (23). We therefore assume that lateral diffusion along the phase II alloys is not rate determining in the present model and proceeds infinitely fast.

The exchange current is obviously a powerful parameter as a measure of the kinetics of the electrochemical hydrogen reaction. Although this parameter is defined in the equilibrium situation it cannot be determined directly under these conditions. I_o can, however, simply be deduced from nonequilibrium measurements (17). Provided that mass transport of the electroactive species in both the solid and electrolyte is not a limiting factor, I_o can be determined by measuring the dependence of the current on the overpotential (η), where η is defined as E-E_e. When η is changed within a small range ($\eta < RT/\alpha nF$) the Butler-Volmer equation can be simplified to

$$I = I_o \frac{F}{RT} \eta \quad [17]$$

Since F/RT is a constant for a given temperature, a linear relationship between the current and the overpotential should be expected. I_o can then be calculated from the slope of such a line (9).

Experimental

The $AB_{5.5}$ melts were prepared by mixing the appropriate amounts of starting materials having a purity of better than 99.9 weight percent (w/o) and arc melting the mixtures under purified argon. Two solidification procedures were employed: the homogeneous melts were cooled down as a button in a copper container or poured out as a thin slab in a massive copper mold; the temperature decrease in this latter case is significantly faster than in the former procedure. The as-produced solid samples were split into two parts: one part was used for material characterization whereas the other part was employed for the electrochemical measurements.

For the material characterization either part was embedded in epoxy resin (Thermosetting Resin-5 from Struers, Denmark) and the surface was subsequently polished in various successive steps. The final polishing step was performed with an OP-S suspension from Struers. The surface morphology was examined qualitatively, using scanning electron microscopy (SEM) and optical microscopy (bright-field mode). In order to distinguish the various crystallographic phases within the solids optically, approximately 250 nm thick Pt-oxide interference layers were additionally sputtered onto the polished surfaces which had previously been cleaned by ion etching for 2 min.

The chemical composition of the polished substrates was determined using electron probe microanalysis (EPMA) with x-ray emission detection which is specific for the chemical elements considered. A qualitative inspection of the elemental distribution is obtained in the scanning mode whereas a more quantitative analysis is obtained when the electron beam is fixed on a small spot. The resolution of this latter method is determined by the penetration depth of the electron beam and is of the order of 0.5 μm at the acceleration voltage used (15 kV). Both methods were employed in this work.

The remaining bulk materials were mechanically ground to a powder. After pulverization only the fraction that passed through a 50 μm sieve was used for the electrochemical measurements. Preceding these measurements, x-ray diffraction analyses were performed on these powders in order to investigate their crystallographic properties. Electrodes were made by mixing the sieved powders with fine copper powder (pro analyse from Merck) in the weight ratio of 1:4 and pressing these mixtures at a pressure of 4×10^8 N · m^{-2} to porous pellets having a diameter

of 8 mm. The weight of the pellets was about 150 mg in all cases. For the electrochemical measurements the pellets were attached to a copper rod of 8 mm diam by a shrink sleeve and were positioned in a double-walled two-compartment cell made of glass, as described in detail by Willems *et al.* (7, 8). As reference a Hg/HgO electrode was used. To reduce the ohmic drop between the working electrode and the reference electrode a Luggin capillary was located close to the hydride forming electrode in the working electrode compartment. All potentials are given with respect to Hg/HgO. A large area Pt electrode was placed in the separate counterelectrode compartment. A porous glass frit provided for the conductivity between the two compartments. The electrolyte was 6*M* KOH (pro analyse from Merck) and was purged of oxygen both before use and during the experiments by bubbling N_2 through the solution. The electrolyte was thermostated within an accuracy of 0.5°C by means of a temperature control unit HS-60 from Huber.

As was pointed out in the theoretical section, it is essential for an appropriate comparison of the exchange currents that the hydrogen content stored in the various electrodes should have a constant value. A constant cathodic current was therefore applied to the previously discharged electrodes until the hydrogen concentration in the solid was 15% of the storage capacity in all cases. Care was taken to ensure that hydrogen gas evolution did not take place during this initial reduction process. After a resting period in which the equilibrium potential was established, I_o was determined at 25°C by changing potentiodynamically ($1\ mV \cdot s^{-1}$) the overpotential within a small range ($\eta = \pm 10$ mV) and measuring the current with a Wenking Potentioscan POS73. It is well known that freshly prepared hydride forming electrodes must be activated for longer times before the optimum electrocatalytic activity is attained. It has been shown that this can easily be achieved by repeatedly charging and discharging the electrodes (7, 28). To exclude these activation phenomena the I_o values were determined at electrodes which were charged and discharged for 180 times at 25°C in all cases.

The galvanostatic charge and discharge experiments were carried out with an automated cycling apparatus. The resulting working electrode potential was continuously recorded. Referring to the nominal storage capacity of the standard alloy [$280\ mAh \cdot g^{-1}$ (7, 8)], the following cycle regime was applied to the electrodes at 25°C: charging for 1 h with a constant cathodic current of $350\ mA \cdot g^{-1}$ through which hydride formation is initiated; resting for 30 s; discharging with a constant anodic current of $350\ mA \cdot g^{-1}$ until the final potential of −550 mV is reached. This potential is chosen so that oxidation of the Cu matrix is amply prevented. After the discharge procedure has been completed, a resting period of 15 min is allowed for the system before the above cycle regime is repeated. The storage capacity [$C(n)$] of the electrodes was determined by integrating the anodic current. The total storage capacity [$C_t(n)$] was measured every thirty cycles by additionally discharging the electrodes with a relatively low oxidation current of $35\ mA \cdot g^{-1}$. The discharge efficiency, which we define as

$$D_{eff} = \frac{C(n)}{C_t(n)} \times 100\% \qquad [18]$$

was also determined under extreme conditions at 0°C after the 180th cycle, using the same cycle regime as described above except that the oxidation current was considerably increased to $840\ mA \cdot g^{-1}$.

Results and Discussion

The surface morphology of two pentary $AB_{5.5}$ compounds is shown in the optical photomicrographs in Fig. 3. The solids were formed from a homogeneous melt having the overall composition of $La_{0.8}Nd_{0.2}Ni_{3.0}Co_{2.4}Si_{0.1}$ during the two solidification procedures described above. Full color optical inspection revealed that a double-phase structure is obtained in both cases. The temperature decrease at which the solidification process was performed has a considerable influence on the size of the crystallites.

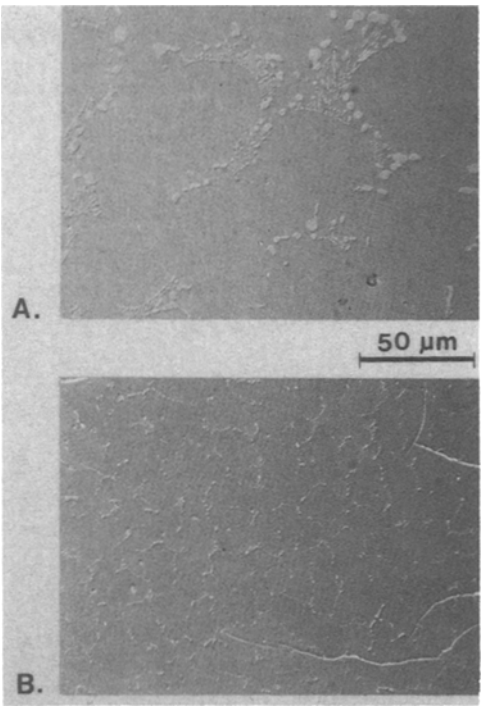

Fig. 3. Optical photomicrographs revealing the surface morphology of two double-phase $AB_{5.5}$ materials formed during the solidification process from a melt with composition $La_{0.8}Nd_{0.2}Ni_{3.0}Co_{2.4}Si_{0.1}$. Both a low (A) and a high (B) solidification rate were used (see Experimental section).

In the case of a moderate temperature decrease (Fig. 3A) the crystallites are in the range of 50-100 µm, whereas much smaller crystallites, in the range of 10-30 µm, are formed when the melt is cooled down more rapidly (Fig. 3B). Clearly, in both preparations a second crystallographic phase decorates the crystallite boundaries. Although this system is much more complex than that of the binary La/Ni system, these results are in agreement with the metallurgical considerations given in the Theoretical section (see Fig. 1). An example of a qualitative EPMA analysis is shown in Fig. 4. This analysis refers to the same material as that investigated in Fig. 3B. The elemental distributions of La, Ni, and Co are shown in Fig. 4B-D, respectively, and were determined by measuring the intensity of their characteristic x-ray radiation. The black dot intensity is a measure of the abundance of the chemical elements and is inversely proportional to the elemental concentration in the solid. The correspondence between the SEM photograph in Fig. 4A and the various elemental distributions is striking. It can be concluded that all elements are depleted in the phase II precipitates with the exception of Co, which has clearly accumulated. Local quantitative analysis of the precipitates revealed an alloy composition of $NiCo_3$. As the penetration depth of the electrons is of the same order of magnitude as the size of the precipitates, the absolute error of this measurement might be quite large. X-ray diffraction measurements on the corresponding powdered materials confirmed, however, that besides the bulk material which is formed by the hydride forming AB_5 compound, having a hexagonal "$LaNi_5$" structure with lattice parameters $a = 5.015$ Å and $c = 3.998$ Å, the second phase has an fcc structure with a lattice parameter of $a = 3.53$ Å, which is indeed in between that of pure Ni and Co (24). In this respect it is important to note that Ni and Co are completely soluble (25). The line broadening related to the Ni/Co precipitates observed in the x-ray diffraction spectra is due either to the small precipitates or to an inhomogeneous distribution of the chemical elements in these precipitates.

A second class of $AB_{5.5}$ compounds, in which Mo was introduced as a foreign chemical element to form a Mo containing phase II alloy, was also investigated. The overall melt compositions of these compounds were

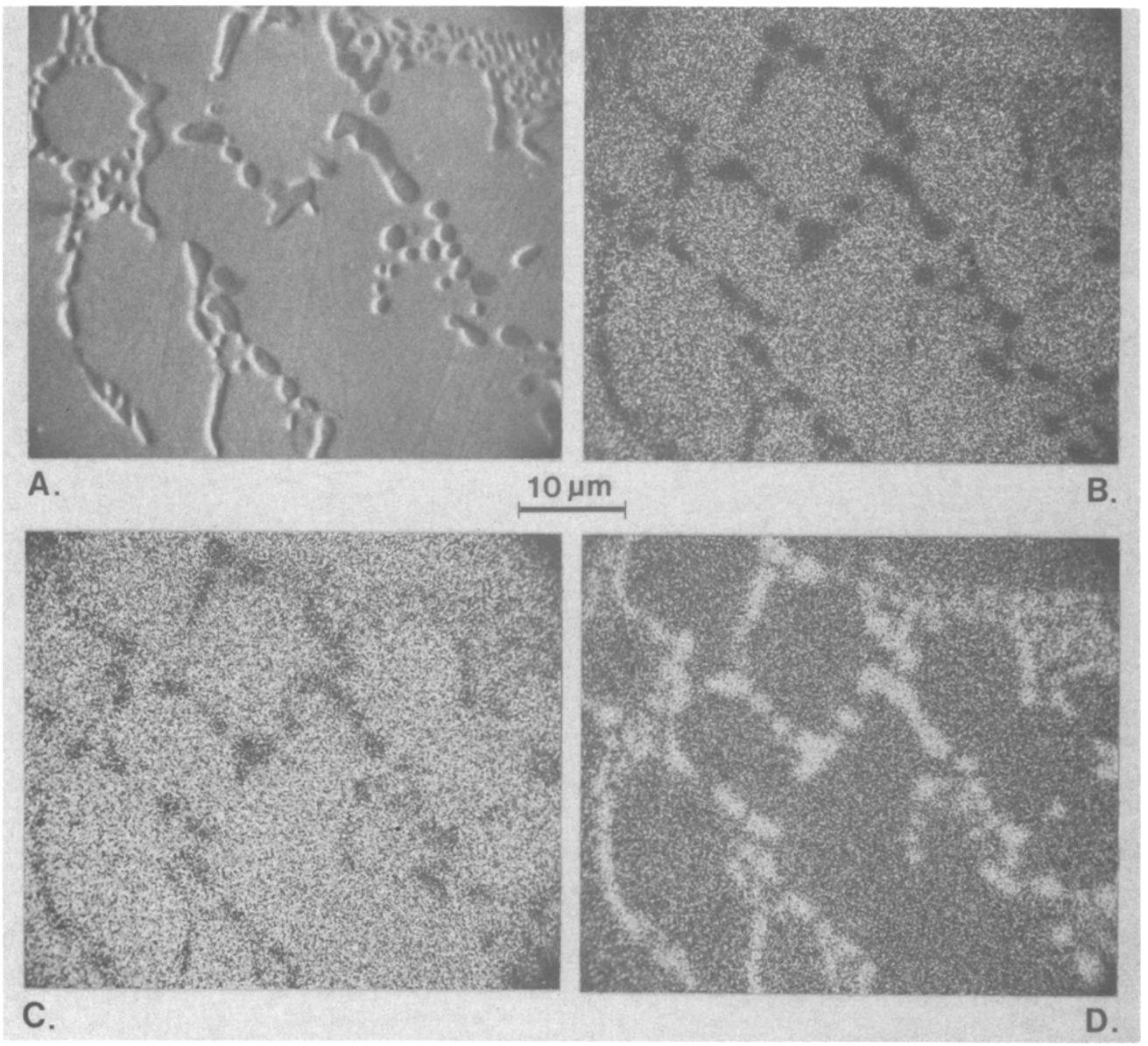

Fig. 4. The elemental distribution in a double-phase solid having an $AB_{5.5}$ composition of $La_{0.8}Nd_{0.2}Ni_{3.0}Co_{2.4}Si_{0.1}$ was determined with EPMA by measuring the element characteristic x-ray radiation and are shown for the elements La, Ni, and Co in (B-D), respectively. The morphology of the corresponding position at the surface is shown in the SEM photograph (A). The melt was cooled down at a high rate.

$$La_{0.8}Nd_{0.2}Ni_{3.0-i}Mo_iCo_{2.4}Si_{0.1} \quad [19]$$

where the Mo content i was varied in the range from 0.05 to 0.30. The desired double-phase structure is formed with $i \leq 0.1$. At larger Mo content inhomogeneous solids containing more than two crystallographic phases are formed. The optimum composition was found with i = 0.1. The surface morphology of this material, formed at a high solidification rate, is very similar to that found for the Mo-free materials (see Fig. 3B) and is shown in Fig. 5. A quantitative EPMA analysis of this material revealed that the correspondence between the surface morphology and the distributions of the various elements within the solid is again excellent, similar to that found in Fig. 4. A representative example of a quantitative EPMA analysis is shown for three elements in the graph of Fig. 6. The elemental concentrations were locally determined at ten different positions lying on a straight line at a mutual distance of 2 μm. The position at the investigated surface was chosen such that one precipitate was located in the middle of this line. It is clear from Fig. 6 that all molybdenum has accumulated in the precipitate together with some Co, whereas Ni is clearly diminished. This latter also holds for the elements La, Nd, and Si. It should again be emphasized that due to the large electron penetration depth with respect to the precipitate size the accuracy with which such small spots can be analyzed is relatively poor. Obviously, this disadvantage does not exist when larger homogeneous regions are analyzed. The composition of the hydride forming phase I could therefore accurately be determined at $La_{0.77}Nd_{0.23}Ni_{2.75}Co_{2.06}Si_{0.11}$ with a relative accuracy of 4%, which is indeed within the reported homogeneity region for AB_5 compounds (18). Furthermore, this result confirms that Mo is not incorporated into phase I. X-ray diffraction analyses of corresponding $AB_{5.5}$ powders revealed that the crystal structure is of the hexagonal $SnNi_3$-type with lattice parameters a = 5.08 Å and c = 4.12 Å. This result in combination with that of the EPMA analyses unequivocally shows that the precipitates consist of $MoCo_3$, the same alloy which was shown to be highly electrocatalytic for the hydrogen reaction (10-13). The small deviations of the lattice parameters with respect to the theoretical values [a = 5.12 Å and c = 4.11 Å (24)] are probably due to the incorporation of a small amount of Ni into the $MoCo_3$ structure. The lattice parameters characteristic for the AB_5 compound were determined to be a = 5.032 Å and c = 3.986 Å.

Although, owing to the complexity of the multicomponent compounds, it is difficult to predict which compound will be precipitated onto the phase I crystallites, some

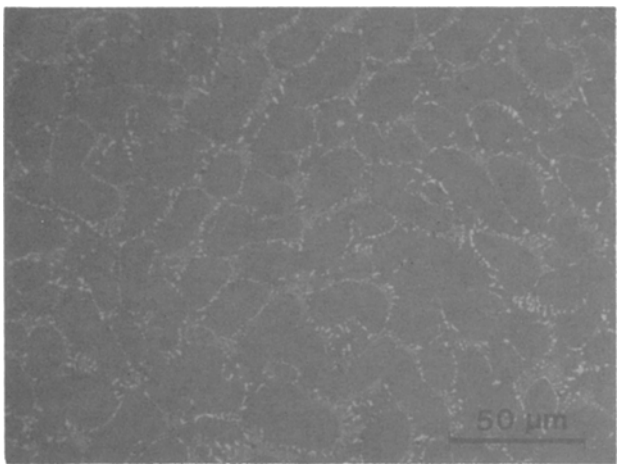

Fig. 5. Optical photomicrograph showing the surface morphology of a double-phase $AB_{5.5}$ compound with overall composition $La_{0.8}Nd_{0.2}Ni_{2.9}Mo_{0.1}Co_{2.4}Si_{0.1}$. A high solidification rate was used.

qualitative thermodynamic remarks can be made. It is obvious from the rather positive value of the enthalpy of formation (ΔH) for $LaMo_5$ [$\Delta H = +25$ kJ · (mole of atoms)$^{-1}$, (26)] that the incorporation of Mo into the AB_5 crystal lattice is unfavorable. On the other hand the ΔH for $MoCo_3$ has a negative value, indicating that the formation of this alloy might be expected beforehand. However, despite the fact that the enthalpy of formation for $MoNi_3$ is even more negative than that of $MoCo_3$ [-8 and -5 kJ. (mole of atoms)$^{-1}$, respectively (26)], the latter compound is finally formed at the grain boundaries at the end of the solidification process. This must be attributed to the better thermodynamic stability of $LaNi_5$ with respect to that of $LaCo_5$ ($\Delta H = -24$ and -15 kJ · (mole of atoms)$^{-1}$, respectively) through which it is easier to withdraw Co from the AB_5 compound than Ni. Thus in order to decide which compound is secreted, it is necessary to take into account not only the thermodynamic stability of the actually formed crystallographic compounds but also that of the compounds which should, in principle, be formed.

The overall exchange currents were electrochemically measured after 180 charge/discharge cycles [I_o(180)]. In all cases a linear dependence was found in accordance with

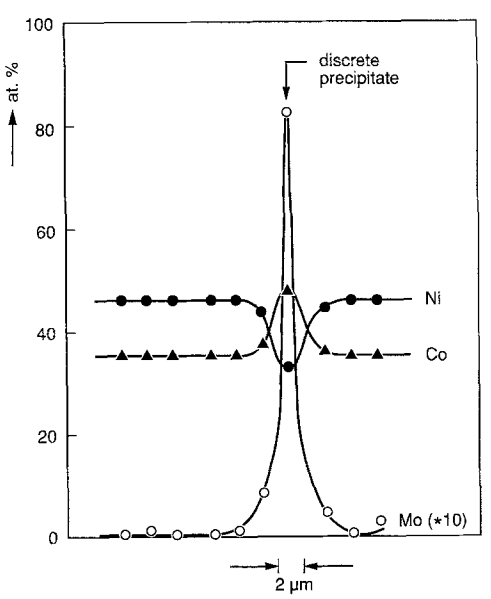

Fig. 6. Atomic concentrations of the elements Ni (●), Co (▲), and Mo (○) as a function of the position at the polished surface of the same $AB_{5.5}$ compound as that shown in Fig. 5. The atomic percentages were determined quantitatively with EPMA at ten successive positions. A discrete phase II precipitate is located in the middle of the plot.

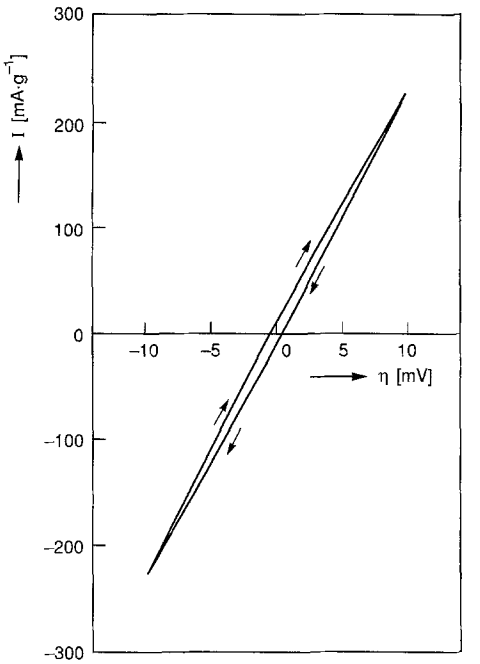

Fig. 7. Potentiodynamic (1 mV · s^{-1}) current-potential curve measured on a double-phase $AB_{5.5}$ electrode with overall alloy composition $La_{0.8}Nd_{0.2}Ni_{2.9}Mo_{0.1}Co_{2.4}Si_{0.1}$ after 180 charge/discharge cycles. Before measuring this current-potential curve the electrode was charged at 15% of its capacity, and a stable equilibrium potential was established. The arrows indicate the scan direction.

the simplified Butler-Volmer equation at small overpotentials. A typical example is given in Fig. 7. According to Eq. [17], I_o can be calculated from the slope of the I *vs.* η curves. The I_o(180) values obtained for the various investigated materials are listed in Table II. This table clearly shows that I_o(180) for the pentary $AB_{5.5}$ compound is significantly larger than the value found for the standard AB_5 alloy (190 mA · g^{-1}). Furthermore it shows that a high solidification rate has a favorable influence on the exchange current: a value of 287 mA · g^{-1} was found at a low rate, whereas 339 mA · g^{-1} was measured at a high solidification rate.

That this latter observation is related to differences in the morphology of both solids can be understood as follows. It has been analyzed that due to repeated cycling with H_2 gas the particle size distribution of AB_5 compounds is terminal, which corresponded with BET measurements performed on these activated powders (27). Similarly, it is likely that after the electrochemical activation process is completed this also holds for the hydride forming compound in the present experiments. This implies that a constant specific surface area is obtained in both cases. It was already concluded from Fig. 3 that due to a higher solidification rate the crystallites and, consequently, the precipitates are much smaller in volume. Obviously, this results in a significant increase of the surface area of the phase II alloy. Since the specific surface area of double-phased materials is composed of A_I and A_{II} (see Eq. [16]), it is clear that when A_{II} of the more electrocatalytic phase II increases at the expense of the less electrocatalytic phase I, this should result in a substantially larger value for I_o. This is in agreement with the experiments (Table I).

Continuing these lines of reasoning, the much higher I_o(180) value for the Mo containing material (588 mA · g^{-1}), also obtained at a high solidification rate, must be attributed to the formation of the highly electrocatalytic $MoCo_3$ alloy. As theoretically predicted (11) and experimentally found (10) the electrochemical rate constant k_{II} must be large for $MoCo_3$ (see Eq. [16]).

Representative results of the cycle life measurements of both $AB_{5.5}$ materials produced at a high solidification rate are shown in Fig. 8 and 9. Curves (a) represent the discharge capacities (C) as a function of the cycle number (n)

Table II. Electrode characteristics, including the exchange current [I_o(180)], the initial [C_t(0)], and remaining [C_t(180)] storage capacities and the corrosion stability [S(400)] for three $AB_{5.5}$ materials are compared with those of the AB_5 standard alloy. The rate at which the smelt is solidified is also indicated.

Overall melt composition	Compound	Solidification rate	I_o(180) (mA · g^{-1})	C_t(0) (mAh · g^{-1})	C_t(180) (mAh · g^{-1})	S(400) (%)
$La_{0.8}Nd_{0.2}Ni_{2.5}Co_{2.4}Si_{0.1}$	(○) AB_5	High	190	293	271	86
$La_{0.8}Nd_{0.2}Ni_{3.0}Co_{2.4}Si_{0.1}$	(▲) $AB_{5.5}$	Low	287	270	261	88
$La_{0.8}Nd_{0.2}Ni_{3.0}Co_{2.4}Si_{0.1}$	(■) $AB_{5.5}$	High	339	276	256	84
$La_{0.8}Nd_{0.2}Ni_{2.9}Mo_{0.1}Co_{2.4}Si_{0.1}$	(●) $AB_{5.5}$	High	588	285	242	73

when an anodic current of 350 mA · g^{-1} is applied to the electrodes. The low capacity, found initially, is due to the activation process of the hydride forming powder, similarly to that reported for many other materials (7, 28). Although the activation period changes from one material to the other, it can be concluded from Fig. 8 and 9 that this process is completed for the various electrodes after a few tens of charge/discharge cycles, indeed long before the exchange currents were measured (at n = 180). The total storage capacity (C_t), obtained by additionally discharging the electrodes with 35 mA · g^{-1} are shown in curves (b) of these figures as a function of n. The straight lines indicate a linear corrosion rate during the first 180 cycles. Extrapolating these lines to n = 0 yields the initial storage capacity C_t(0). These electrode characteristic values are also listed in Table II together with the values obtained for the corrosion stability which was defined by Eq. [1]. As expected, all initial storage capacities are only slightly smaller than that found for the standard alloy, since only the phase I alloy is able to form a hydride. The corrosion stabilities of the various materials are also very similar to that of the standard alloy. Only the S(400) value for the Mo containing material deviates somewhat. This must very likely be attributed to the higher Ni content in the phase I compound which, according to the EPMA analyses, was determined to be $Ni_{2.75}$ whereas the optimum composition was found to be at $Ni_{2.5}$ (7, 8). Inspection of Table I indeed reveals that the corrosion stability is inversely proportional to the Ni content. By fine tuning the overall melt composition, this can very likely be improved, so that the corrosion rate is expected to decrease to the value corresponding to that of the standard alloy (Table I).

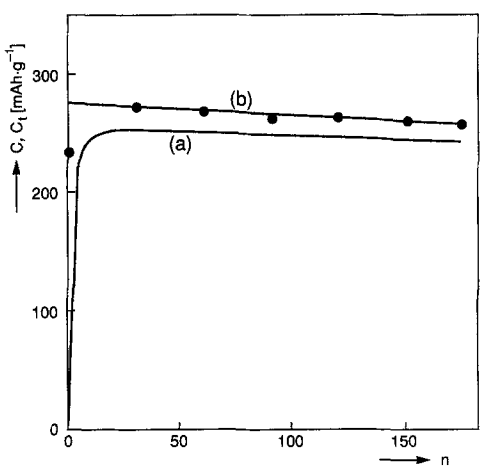

Fig. 8. The storage capacity (C) as a function of charge/discharge cycles (n) is shown in curve (a) for an $AB_{5.5}$ electrode with composition $La_{0.8}Nd_{0.2}Ni_{3.0}Co_{2.4}Si_{0.1}$; the double-phase structure is produced with a high solidification rate. Both the charge and discharge current was 350 mA · g^{-1}. The total storage capacity (C_t) is measured with an additional discharge current of 35 mA · g^{-1} [curve (b)].

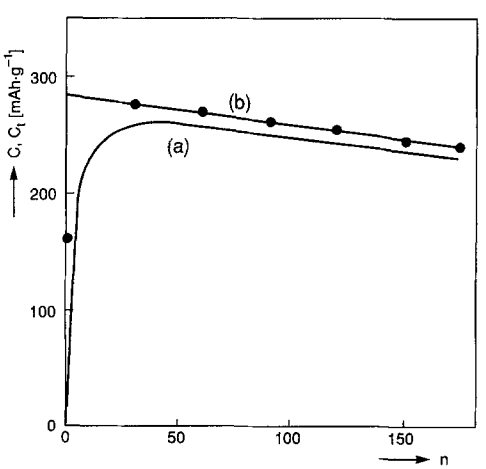

Fig. 9. The same experiment as in Fig. 8 for the Mo containing alloy: $La_{0.8}Nd_{0.2}Ni_{2.9}Mo_{0.1}Co_{2.4}Si_{0.1}$.

We have shown by measuring the exchange current that the electrocatalytic activity of the considered double-phase materials is significantly higher than that of the standard alloy. This should obviously have consequences for the rate at which these electrodes can be electrochemically charged and discharged. Clearly, the additional amount of charge released from the electrodes, resulting from low current discharge, (C_t-C), is related to the electrocatalytic activity. Figure 10 shows this relationship after 180 charge/discharge cycles for the four materials listed in Table II. Although the discharge efficiency is relatively large ($D_{eff} \geq 89\%$) for all electrodes under these moderate conditions, there is a considerable decrease of (C_t-C), resulting from the higher I_o values (see Fig. 10).

It is evident that the improved electrocatalytic surface activity of the materials will show its full advantage when the electrodes are cycled under more extreme conditions. We therefore determined the discharge efficiency of the electrodes by means of Eq. [18] after n = 180 at an electrolyte temperature of 0°C and using a much higher discharge current (840 mA · g^{-1}). The relation between D_{eff} (under these extreme conditions) and I_o is represented in Fig. 11.

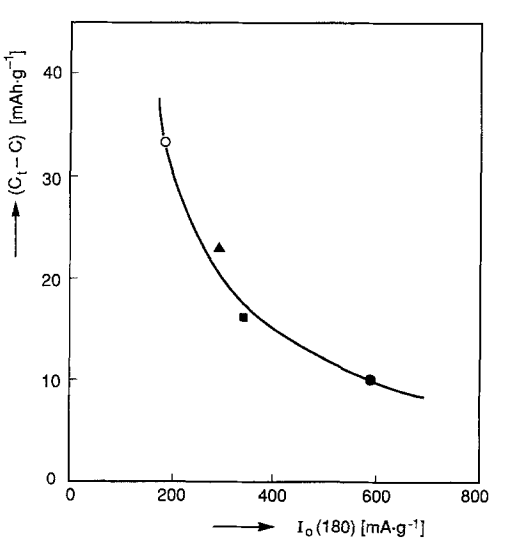

Fig. 10. The additional discharge capacity (C_t-C) resulting from low current discharge at n = 180 as a function of the exchange current [I_o(180)] at 25°C for the four materials listed in Table II: standard $AB_{5.5}$ alloy (○); pentary $AB_{5.5}$ alloys (▲, ■); sextary $AB_{5.5}$ alloy (●).

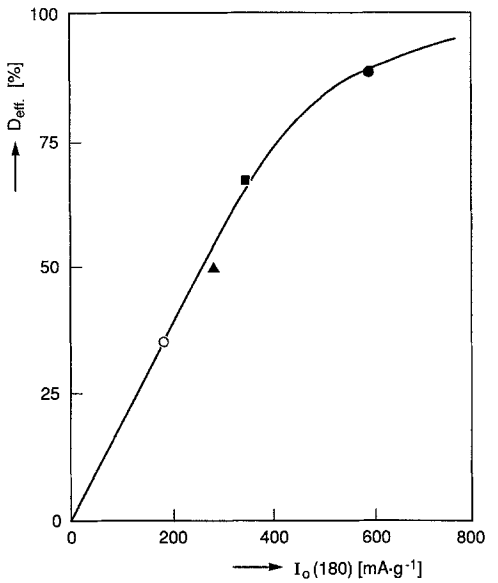

Fig. 11. The discharge efficiency (D_{eff}) determined according to Eq. [18] under the extreme conditions of 0°C and a high discharge current of 840 mA · g^{-1} as a function of the exchange current [I_o(180)] for the standard alloy (○), the pentary $AB_{5.5}$ alloys (▲, ■), and the Mo containing $AB_{5.5}$ alloy (●).

It shows that the discharge efficiency increases significantly with increasing I_o, as expected. In contrast to the very low efficiency generally found for the standard alloy (34%), which corresponds with a low I_o value, a dramatic improvement up to 90% is achieved to the most electroactive, $MoCo_3$-based, material. This shows that these latter double-phase materials are very attractive as rechargeable hydride forming electrodes with fast charge/discharge characteristics even under extreme conditions.

Conclusions

On the basis of a working model we have shown that it should theoretically be possible to improve the electrocatalytic activity of hydride forming materials by making use of double-phase compounds. These compounds were proposed to consist of a single-phase hydride forming material of the AB_5 type and a second, highly electrocatalytic, phase which is homogeneously distributed upon the powder particles. This phase II alloy should be composed of the appropriate combination of transition metals for which, according to the Brewer-Engel valence bond theory, synergistic effects are reported for the kinetics of the electrochemical hydrogen reaction. Experimental evidence supporting this model has been presented in this paper. It has been shown that double-phase solids with the desired morphology can be easily produced simply by solidifying a melt with $AB_{5.5}$ composition; a composition just outside the homogeneity region of AB_5 alloys. Two different $AB_{5.5}$ systems were investigated. The electrocatalytic activity of these systems, which was characterized by the overall exchange current, was found to be significantly higher than that of corresponding single-phase AB_5 compounds. The solidification rate of the melt was found to have a marked influence on the size of the crystallites. Smaller crystallites, obtained at higher solidification rates, show a favorable influence on the surface kinetics.

We suggest that the method employed in this work to improve the kinetics of hydride formation has a much wider relevance and should not be restricted to the class of AB_5 compounds described in this paper. It seems likely that it can be expanded to other classes of hydride forming materials (4). Furthermore, other reported "synergistic compounds" (10-13) might also successfully be employed as phase II alloys. This might be of special importance in the near future as these double-phase materials seem to be very attractive for use in rechargeable Ni-hydride batteries with extremely fast charge/discharge characteristics.

Acknowledgments

The authors thank Mr. H. C. Donkersloot and Mrs. W. Gijsbers for the preparation and polishing of the intermetallic compounds. Mr. J. H. T. Hengst is acknowledged for the EPMA analyses and Mr. J. L. C. Daams for the x-ray analyses. They are also grateful to Mr. J. E. A. M. van den Meerakker and Dr. L. Fokkink for helpful discussions.

Manuscript submitted June 22, 1990; revised manuscript received Jan. 25, 1991.

Philips Research Laboratories assisted in meeting the publication costs of this article.

REFERENCES

1. H. Zijlstra and F. F. Westendorp, *Solid State Comm.*, **7**, 857 (1969).
2. J. H. N. van Vucht, F. A. Kuijpers, and H. C. A. M. Bruning, *Philips Res. Rep.*, **25**, 133 (1970).
3. F. A.Kuijpers, *Philips Res. Rep. Suppl.*, No. 2 (1973).
4. K. H. J. Buschow, P. C. P. Bouten, and A. R. Miedema, *Rep. Prog. Phys.*, **45**, 937 (1982).
5. P. A. Boter, U.S. Pat. 4,004,943 (1977).
6. H. J. H. van Deutekom, U.S. Pat. 4,214,043 (1980) and 4,312,928 (1982).
7. J. J. G. Willems, *Philips J. Res. Suppl.*, **39**(1), 1 (1984).
8. J. R. van Beek, J. J. G. Willems, and H. C. Donkersloot, in Proceedings of 14th International Power Sources Symposium, "Power Sources 10," L. J. Pearce, Editor, p. 317 (1985).
9. P. H. L. Notten and E. Brok, Extended Abstract 5.13, 38th ISE Meeting, Maastricht (1987).
10. C. M. Lačnjevac and M. M. Jakšić, *J. Res. Inst. Catalysis, Hokkaido Univ.*, **31**, 7 (1983).
11. M. M. Jakšić, *Electrochim. Acta*, **29**, 1539 (1984).
12. M. M. Jakšić, *Int. J. Hydrogen Energy*, **11**, 519 (1986).
13. M. M. Jakšić, *ibid.*, **11**, 727 (1987).
14. H. Wendt and V. Plzak, *Electrochim. Acta*, **28**, 27 (1983).
15. H. Kita, *This Journal*, **113**, 1095 (1966).
16. H. Yayama, K. Kuroki, K. Hirakawa, and A. Tomokiyo, *Jpn. J. Appl. Phys.*, **23**, 1619 (1984).
17. K. J. Vetter, "Electrochemical Kinetics," Academic Press, Ltd., London (1967).
18. K. H. J. Buschow and H. H. van Mal, *J. Less-Common Met.*, **29**, 203 (1972).
19. T. Erdey-Grüz, "Kinetics of Electrode Processes," Adam Hilger, Ltd., London (1970).
20. H. Yayama, K. Hirakawa, and A. Tomokiyo, *Jpn. J. Appl. Phys.*, **25**, 739 (1986).
21. A. W. Adamson, "Physical Chemistry of Surfaces," 2nd ed., Interscience, London (1967).
22. W. E. Wallace, R. F. Karlicek, Jr., and H. Imamura, *J. Phys. Chem.*, **83**, 1708 (1979).
23. L. Schlapbach, A. Seiler, F. Stucki, and H. C. Siegmann, *J. Less-Common Met.*, **73**, 145 (1980).
24. P. Villars and L. D. Calvert, in "Pearson's Handbook of Crystallographic Data for Intermetallic Phases," ASM, Metals Park, OH (1985).
25. M. Hansen, "Constitution of Binary Alloys," 2nd ed. p. 485, McGraw-Hill, Ltd., London (1958).
26. F. R. de Boer, R. Boom, W. C. M. Mattens, A. R. Miedema, and A. K. Niessen, "Cohesion in Metals, Transition Metal Alloys," North Holland Comp., Amsterdam (1988).
27. H. H. van Mal, Philips Res. Rep. Suppl. No. 1 (1976).
28. H. Yayama, O. Ichinomiya, and K. Hirakawa, *Jpn. J. Appl. Phys.*, **22**, L621 (1983).